Available online at www.sciencedirect.com
ScienceDirect
International Journal of Heat and Fluid Flow 27 (2006) 789–799
International Journal of HEAT AND FLUID FLOW
www.elsevier.com/locate/ijhff

Approximate near-wall treatments based on zonal and hybrid RANS–LES methods for LES at high Reynolds numbers

F. Tessicini, L. Temmerman [1], M.A. Leschziner *

Department of Aeronautics, Imperial College London, South Kensington Campus, Prince Consort Road, London SW7 2AZ, UK

Received 17 October 2005; received in revised form 18 January 2006; accepted 4 March 2006
Available online 30 June 2006

Abstract

Two strategies, combining a LES scheme with different near-wall RANS approximations, are investigated by reference to simulations for plane channel flow and two separated flows at moderate and high Reynolds numbers, respectively. One strategy is a hybrid modelling scheme, wherein the subgrid-scale model in the outer LES domain is interfaced with a RANS model in a predefined near-wall layer. The other is a zonal method in which a thin-shear-flow RANS solution in the near-wall layer, embedded within the LES domain which covers the entire flow, is used to provide boundary conditions for the LES computation, the two thus being loosely coupled. Both methods allow the thickness of the near-wall RANS layer to be chosen freely. In the hybrid LES–RANS scheme, the near-wall layer is interfaced to the outer LES region, subject to compatibility conditions for velocity and turbulent viscosity imposed across the interface. These conditions are extracted dynamically as the simulation progresses. In the zonal approach, a mixing-layer model provides the eddy-viscosity field in the near-wall layer, while in the hybrid approach, a two-equations (k–ϵ) model is used.

Keywords: Turbulent flow; Hybrid LES–RANS; Zonal model; Two-layer model; Near-wall simulation

1. Introduction

Large eddy simulation is now almost routinely used to investigate fundamental aspects of turbulence mechanics, to help validate statistical closures and to obtain predictions for flows in which unsteady events associated with turbulence are of major interest or influence. Although LES continues to be an expensive approach at practically relevant Reynolds numbers, the expense is tolerable when the flow being simulated is remote from walls. However, flows which are substantially affected by near-wall shear and turbulence pose serious resource challenges as a consequence of the need to increase the near-wall grid resolution broadly in line with $N \propto Re^{1.8}$, in order to restrict the distance between the wall and the nodes closest to the wall to around $y^+ = 2$ and to also maintain a near-wall cell-aspect ratio within $\Delta y^+/\Delta s^+ \approx 1/50$, where s is the mean flow direction close and parallel to the wall. Thus, at high Reynolds numbers, the utility of LES in the practical environment depends greatly on the availability of acceptably accurate near-wall approximations that allow the resolution requirements to be reduced to economically tenable levels. Over the past few years, a whole range of approaches to this problem have been proposed. These include log-law-based wall-functions, investigated extensively by Temmerman et al. (2003) for separated flow, various zonal and seamless RANS–LES hybrid schemes, notably the DES method of Spalart (2000) and the two-layer method examined by Balaras et al. (1996). So far, no one particular method has been demonstrated to be definitively superior to others, and all involve restrictions and limitations which adversely affect the resulting solution in some circumstances. Even in a simple, fully-developed channel flow at high Reynolds number, no method is able to give a solution that is without defect in the vicinity of the

* Corresponding author. Fax: +44 20 758 48120.
E-mail address: mike.leschziner@ic.ac.uk (M.A. Leschziner).
[1] Present address: Numeca International s.a. Av. F. Roosevelt 5 B-1050 Brussels, Belgium.

0142-727X/$ - see front matter © 2006 Elsevier Inc. All rights reserved.
doi:10.1016/j.ijheatfluidflow.2006.03.024

edge of the near-wall layer within which the approximate model is applied.

In earlier work by Temmerman et al. (2002, 2005) and Hanjalić et al. (2003), a RANS–LES hybrid method has been investigated, in which a conventional low-Reynolds-number one-equation k–l RANS model is applied within a near-wall layer, the thickness of which can be chosen freely. Coupling to the LES domain is effected via compatibility constraints, including a dynamic process wherein the turbulent viscosity at the RANS side of the interface is adjusted by reference to the subgrid-scale viscosity in the LES region. In the present paper, this methodology is implemented in combination with a two-equation k–ϵ model in the near-wall layer and a one-equation subgrid-scale model in the LES region. To permit this, an implicit solution method of the turbulence equations within the layer had to be devised to procure stability and boundedness.

In a second 'zonal' approach pursued in parallel, the near-wall layer is numerically separated from the LES domain. Simplified (parabolized) versions of the momentum equations are solved in the layer, together with the turbulence-model equations (at this stage, a mixing-length model) with 'boundary conditions' taken from the outer LES domain at the interface. The solution provides the wall-shear stress, which is then imposed as a boundary condition on the LES domain. This is, essentially, an application of the method of Balaras et al. (1994), Cabot (1995) and Wang and Moin (2002), here within a body-fitted finite-volume framework. Both methods are contrasted against each other, as well as against a log-law-based wall-function approach. Their performance is examined by reference to a fully-developed channel flow at $Re =$ 42,200, a spanwise homogeneous, separated flow in a channel which is constricted by hill-shaped protrusions on one wall at $Re = 21{,}560$, and a spanwise homogeneous flow separating from rear upper side of a hydrofoil at a chord Reynolds number of $Re_c = 2.2 \times 10^6$.

2. Outline of LES–RANS strategies

2.1. The hybrid strategy

The principles of the hybrid scheme are conveyed in Fig. 1(a). The following provides a summary of a more detailed description provided by Temmerman et al. (2005). Within sensible limits, dictated by the requirement that the flow in the near-wall layer be shear-dominated and of low curvature, the thickness of the near-wall layer may be chosen freely, in principle, although in applications to follow, the layer is simply bounded by a particular wall-parallel grid surface. The LES and RANS regions are bridged at the interface by interchanging velocities, modelled turbulence energy and turbulent viscosity, the last being subject to the continuity constraint across the interface, $\nu_{\mathrm{LES}}^{\mathrm{mod}} = \nu_{\mathrm{RANS}}^{\mathrm{mod}}$. Turbulence in the RANS layer is here represented by means of the two-equation model of Lien and Leschziner (1994). With the turbulent viscosity given by $\nu_t = C_\mu f_\mu k^2/\varepsilon$, matching the subgrid-scale viscosity to the RANS viscosity at the interface implies:

$$C_{\mu,\mathrm{int}}^{\mathrm{av}} = \frac{\langle \nu_{\mathrm{LES}}^{\mathrm{mod}} \rangle}{\langle f_\mu k^2/\varepsilon \rangle}, \tag{1}$$

where $\langle\cdot\rangle$ indicates an averaging operation, which may be effected over any homogeneous direction, a predefined patch or over time. In fact, Temmerman et al. (2005) show, by reference to simulations for channel flow at $Re_\tau = 2000$, that the use of the instantaneous value of $C_{\mu,\mathrm{int}}$, rather than an averaged value, can be advantageous in that it diminishes the characteristic inflection in the log-law region close to the interface, attributed to the 'spectral enrichment' around the interface that arises as a result of the highly unsteady value of $C_{\mu,\mathrm{int}}$ being imposed onto the RANS layer. On the other hand, this increased unsteadiness goes counter to the fundamental objective of reducing the resolved component in the near-wall layer and delegating the representation of the turbulence activity to the RANS model. Boundary conditions for solving the k-equation in the RANS layer are provided by the subgrid-scale energy in the LES domain, while the dissipation rate is evaluated from the subgrid-scale energy as $k^{1.5}/(Const. \times \Delta)$ where Δ represents the cell size $(\Delta x \Delta y \Delta z)^{1/3}$. The turbulence equations in the sublayer are solved by a coupled, implicit strategy, replacing an earlier sequential, explicit solution applied to one-equation models, which was found to cause stability problems with two-equation models. The smooth transition from the RANS value $C_\mu = 0.09$, presumed to apply at the wall, to the interface value $C_{\mu,\mathrm{int}}$ is effected by the empirical exponential function (see Temmerman et al., 2005):

$$C_\mu = 0.09 + (C_{\mu,\mathrm{int}}^{\mathrm{av}} - 0.09)\frac{1 - \exp(-y/\Delta)}{1 - \exp(-y_{\mathrm{int}}/\Delta_{\mathrm{int}})} \tag{2}$$

Based on the work of Yoshizawa and Horiuti (1985), a one-equation model has been used to determine the subgrid-scale stresses in the LES region. This evaluates the subgrid-scale turbulence energy from the transport equation:

$$\frac{\partial k}{\partial t} + \frac{\partial u_j k}{\partial x_j} = \frac{\partial}{\partial x_j}\left[(\nu + \nu_t)\frac{\partial k}{\partial x_j}\right] + P_k - \epsilon_k, \tag{3}$$

where

$$P_k = 2\nu_t S_{ij} S_{ij}, \quad \nu_t = C_\nu \Delta k^{\frac{1}{2}}, \quad \epsilon_k = C_\epsilon \frac{k^{\frac{3}{2}}}{\Delta}$$

from which the subgrid-scale stresses are determined via the usual linear Boussinesq stress–strain relationship. Yoshizawa and Horiuti originally suggested the values $C_\nu = 0.04$ and $C_\epsilon = 1.0$ for the constants in the above equation, and these were adopted by Temmerman et al. (2005) in their studies of the present hybrid scheme, but within a version that incorporated a one-equation RANS model in the near-wall layer. However, Dahlström (2003) reports the set $C_\nu = 0.07$ and $C_\epsilon = 1.05$ as yielding better results

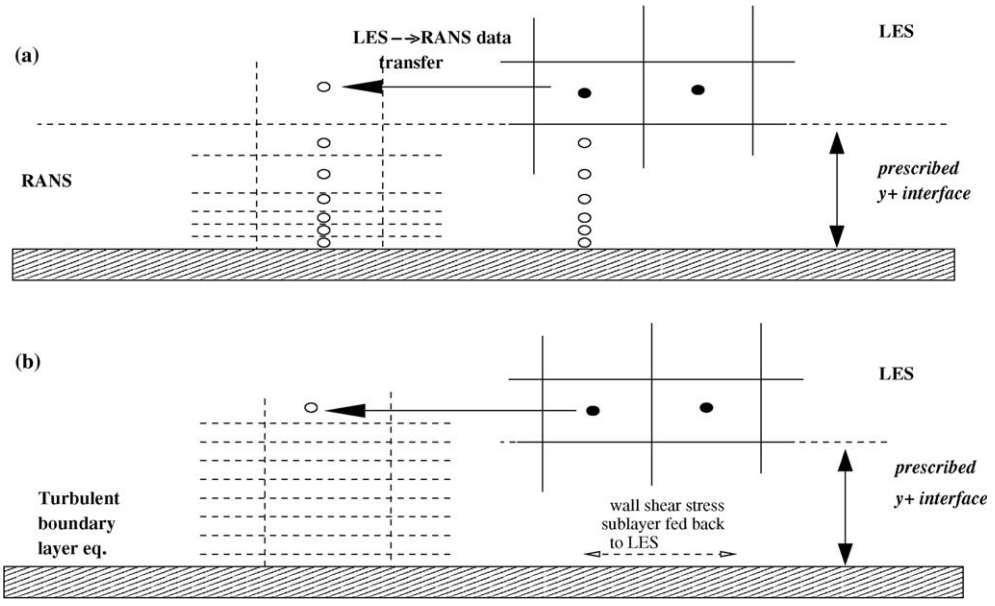

Fig. 1. Schematics of (a) the hybrid LES/RANS scheme; and (b) the two-layer method.

in channel flow, and these were thus adopted in the present work. Subject to the assumption of turbulence equilibrium, $P_k = \epsilon_k$, the different sets of constants may readily be shown (see Hamba, 2001) to imply different values for the Smagorinsky constant, via the resulting relationship:

$$C_s^2 = \frac{C_v^{3/2}}{C_\epsilon^{1/2}}, \tag{4}$$

where C_s is the Smagorinsky constant. Thus, $C_v = 0.07$ and $C_\epsilon = 1.05$ yield $C_s = 0.134$; while $C_v = 0.04$ and $C_\epsilon = 1.$ result in $C_s = 0.09$.

The implications of the differences in the constants are explored below, briefly, by reference to a study of the decay of homogeneous isotropic turbulence in a periodic box, with a 512^3-nodes DNS data set serving as the benchmark. Three simulations were performed, one with the dynamic model of Germano et al. (1991) and two with the one-equation SGS model incorporating the two sets of constants stated above. The DNS tracked the decay of turbulence from $Re_\lambda = 945$ to $Re_\lambda = 60$, Re_λ being the Taylor micro-scale Reynolds number. The AGARD data set (see Wray, 1998) includes a flow field, filtered to a resolution of 128^3, with an energy spectrum corresponding to $Re_\lambda = 104.5$. At this value, any unphysical features remaining from the prescription of synthetic turbulence as the starting condition for the DNS were held to be insignificant. This field was thus used as the initial condition for the LES performed herein on a 64^3 computational mesh. Results are compared against the DNS data in Fig. 2. The left-hand-side plot shows the decay of turbulence energy with time, where $t^* = (t - t_0)L/k_0$, with L being the box side, k_0 the initial kinetic energy and t_0 the time at which $Re_\lambda = 104.5$. All LES solutions agree fairly well with the DNS data, the one-equation model with the original constants giving a rate of decay closest to the DNS, except for the final stage for which the set $C_v = 0.07$ and $C_\epsilon = 1.05$ gives better agreement. However, the energy spectra, shown on the right-hand-side plot for $t^* = 0$, 0.2 and 0.7, indicate that the original set leads to a pile-up of energy in the high-frequency range, which suggests insufficient dissipation. On the other hand, Dahlström's set gives a slightly excessive dissipation. Hence, the implication is that the most appropriate set would lie somewhere between the two.

2.2. The zonal two-layer strategy

The objective of a zonal strategy is to provide the simulation with the wall-shear stress, using information from the outer flow near the wall. The wall-shear stress can be determined from an algebraic law-of-the-wall model or from differential equations solved on a near-wall-layer grid refined in the wall-normal direction—an approach referred to as "two-layer wall modelling". In geometrically simple flows, such as that in a channel, the wall-parallel velocity can be fitted to the log law to predict a wall-shear stress, the simplest form being:

$$U_m = u_\tau/\kappa * \ln(y_m u_\tau/\nu) + B. \tag{5}$$

This is the basis of using wall functions in LES, and a variety of related forms have been examined by Temmerman et al. (2003).

The two-layer wall method, shown schematically in Fig. 1(b), was originally proposed by Balaras et al. (1994) and tested by Balaras et al. (1996) and by Wang and Moin (2002) to calculate the flow over the trailing edge of a hydrofoil. At solid boundaries, the LES equations are solved up to a near-wall node that is located, typically, at $y^+ = 50$. From this node to the wall, a refined mesh is embedded into the main flow, and the following simplified turbulent boundary-layer equations are solved:

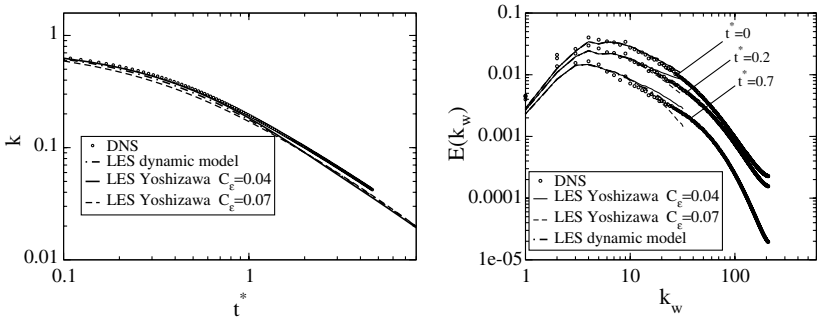

Fig. 2. Decay of turbulent kinetic energy and spectra of the resolved energy for the case of homogeneous isotropic box turbulence; comparisons between LES with $64\times64\times64$ and DNS with $512\times512\times512$ nodes.

$$\frac{\partial}{\partial x_n}\left[(\nu+\nu_t)\frac{\partial \overline{u_i}}{\partial x_n}\right]=F_i,$$
$$F_i=\frac{\partial \overline{u_i}}{\partial t}+\frac{\partial \overline{u_j}\,\overline{u_i}}{\partial x_j}+\frac{\partial \bar{p}}{\partial x_i}, \tag{6}$$

where n denotes the direction normal to the wall and i identify the wall-parallel directions. In the present study, only the pressure-gradient term has been included in F_i. The effects of including the remaining terms are being investigated and will be reported in a future paper. However, order-of-magnitude considerations suggest that the effect of these terms is small for relatively thin near-wall layers. The eddy viscosity ν_t is here obtained from a mixing-length model with near-wall damping, as done by Wang and Moin, 2002:

$$\frac{\nu_t}{\nu}=\kappa y^+\left(1-e^{-\frac{y^+}{A^+}}\right)^2, \tag{7}$$

where y^+ is the distance in wall units based on the local, instantaneous friction velocity, $\kappa=0.4$ and $A^+=19$, the latter found to give an approximately correct rate of wall-asymptotic decay of the viscosity. The boundary conditions for Eq. (6) are given by the unsteady outer-layer solution at the first grid node outside the wall layer and the no-slip condition at $y=0$. Since the friction velocity u_τ is required in Eq. (7) to determine y^+ (which depends, in turn, on the wall-shear stress given by Eq. (6)), an iterative procedure had to be implemented, wherein ν_t is calculated from Eq. (7), followed by an integration of Eq. (6).

3. Fully-developed channel flow

The performance of the present near-wall practices is first assessed by reference to a turbulent channel flow at a Reynolds number of 42,200, based on half-channel width and bulk velocity, for which the wall-friction Reynolds number, Re_τ, is 2000. The computations are summarised in Table 1, and related solutions are presented in Fig. 3. The table also lists the modelling practices adopted and the location of the interface. Thus: 'Ref. LES' identifies a highly-resolved reference solution; '1EQ' and '2EQ' denote, respectively, that a one-equation (k–l) and the two-equation (k–ϵ) model have been used in the RANS

Table 1
Grids, modelling practices and interface locations used for channel-flow simulations

Case	Grid	SGS model	Interface (y^+)
Ref. LES	$512\times128\times128$	WALE	–
2EQ-*j*17	$64\times64\times32$	k-eq	113
1EQ-*j*17	$64\times64\times32$	k-eq	113
Two-layer $F_i=0$	$64\times64\times32$	WALE	60
log-Law WF	$64\times64\times32$	WALE	60

layer; '*j*17' relates to the grid line at which the interface has been placed, and this corresponds to the wall distance identified in the last column; and 'WALE' and 'k-eq' signify the subgrid-scale models used (Nicoud and Ducros, 1999; Yoshizawa and Horiuti, 1985, respectively). Both the hybrid and two-layer-model simulations were performed on a domain of $2\pi h\times2h\times\pi h$. For the hybrid RANS–LES method, the near-wall-cell dimensions were $\Delta x^+=\Delta z^+=196$ and $\Delta y^+=0.8$, while the wall-normal cell height for the two-layer approach was $\Delta y^+=60$, the other two dimensions remaining unchanged. Thus, the cells have an aspect ratio $\frac{\Delta x^+}{\Delta z^+}=1$, in accordance with a recommendation by Shur et al. (1999). For the highly-resolved LES computation ('Ref. LES'), the dimensions of the near-wall cells were $\Delta x^+=\Delta z^+=24.5$ and $\Delta y^+=1.5$.

The velocity profiles given in Fig. 3 indicate fairly close agreement between the solutions derived from the two-layer and hybrid schemes, on the one hand, and the highly-resolved LES solution, on the other. All profiles feature inflections, which are almost always observed with this type of approximations, and these signify insufficient turbulence activity (resolved + modelled) in the interface region. Of the solutions, those arising from the wall-function and the two-layer implementations are virtually identical (represented by a single visible curve closest to the reference solution). This is not surprising, for the latter is a 'sublayer-resolving' version of the former, both operating within layers of identical thickness. The solution obtained with the one-equation hybrid scheme is furthest from the highly-resolved solution, but here the interface is at $y^+=113$, relative to 'only' 60 for the two-layer scheme. However, the two-equation form gives an improved solution, which is quite close to the reference profile. The

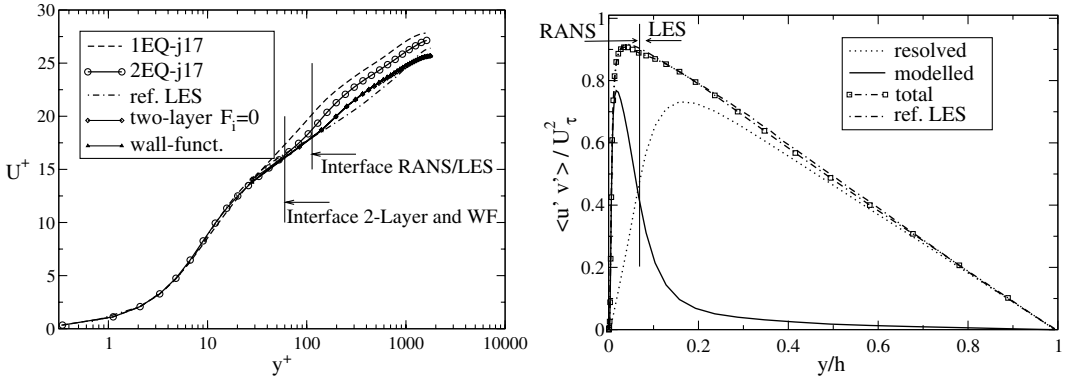

Fig. 3. Profiles of velocity (left-hand side) and shear stress (right-hand side) for channel flow at $Re = 42{,}200$; Ref. LES with $512 \times 128 \times 128$ nodes, relative to $64 \times 64 \times 32$ for the wall approximations.

shear-stress plot shows, for the two-equation hybrid method, that the modelled proportion of the total shear stress rises rapidly towards the wall to a peak of almost 80% of the maximum. This is consonant with the objective of such a method, namely to delegate an increasing proportion of the turbulence activity to the statistical model as the wall is approached.

4. Constricted-channel flow

The near-wall approximations are next contrasted for the case of a channel with periodically arranged hill-shaped constrictions along one wall, which cause massive separation at their leeward side. The computational domain is $9h \times 3.036h \times 4.5h$, with h being the hill height, and extends from one hill crest to the next (see Fig. 4), with periodic conditions applied at both ends. The Reynolds number, based on the flow rate, is 21,560. This value is rather low, making this flow a less than ideal test case. However, there are very few alternative flow configurations at higher Reynolds numbers for which there are benchmark solutions. An extensive study of this flow, with particular emphasis on the sensitivity to wall functions and SGS models, is reported in Temmerman et al. (2003). The availability of extensive data from two highly-resolved simulations over a grid of about 5 million cells allows the accuracy of the present approximate methods to be assessed. This computation forms the first entry in Table 2. Five simulations with approximate near-wall methods are reported: three with the hybrid scheme, with different interface locations, one with the two-layer scheme and the fifth with the log-law wall function. The inclusion of the pressure gradient in the two-layer scheme reflects the expectation that the large variations of streamwise pressure caused by the hill geometry are influential. The WALE SGS model was used in the Ref. LES calculation, the wall-function simulation and in conjunction with the two-layer approach, while the one-equation model of Yoshizawa and Horiuti (1985) was adopted for the hybrid scheme. All were performed with substantially coarser grids than that of the reference solution, but there are significant differences in respect of the wall-normal grid between the meshes used for the hybrid and two-layer methods, because the former requires the grid to be wall-resolving in the wall-normal direction. The resolution of the grid in the streamwise direction is equivalent to that of the coarsest grid used in Temmerman et al. (2003) for the study of wall-functions. The spanwise resolution was chosen to keep the ratio $\Delta x^+/\Delta z^+$ as close

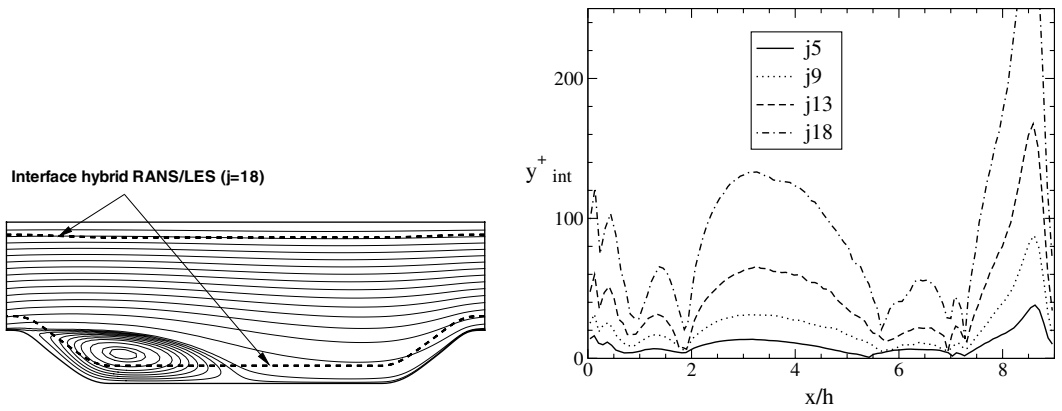

Fig. 4. Location of upper and lower-wall interfaces $j18$ for the constricted channel flow (left-hand side) and distributions of y^+ along the lower-wall interfaces $j5$–$j18$ (right-hand side).

Table 2
Grids, separation and reattachment points and interface locations for constricted-channel simulations

Case	Grid	$(x/h)_{sep}$	$(x/h)_{reat}$	SGS	Interface (j)
Ref. LES	$196\times128\times186$	0.22	4.72	WALE	–
2EQ-$j5$	$112\times64\times56$	0.25	5.43	k-eq	5
2EQ-$j13$	$112\times64\times56$	0.23	5.76	k-eq	13
2EQ-$j18$	$112\times64\times56$	0.23	5.69	k-eq	18
Two-layer $F_i=\frac{\partial p}{\partial x_i}$	$112\times64\times56$	0.42	5.12	WALE	5
log-Law WF	$112\times64\times56$	0.58	3.05	WALE	5

to unity as possible, and this thus gives a much coarser grid than the one used in the reference computation. The configuration sketch in Fig. 4 contains dashed lines that indicate the physical location of the interfaces corresponding to "$j18$", the 4th entry in Table 2. Fig. 4 also gives the distribution of the universal wall distance between the hill wall and the wall-nearest grid surface. As seen, typical y^+ values are 10, 30, 50 and 100 for the interface locations $j5$, $j9$, $j13$ and $j18$, respectively. As seen in Fig. 4, the last ($j18$) extends almost to the centre of the recirculation zone.

Table 2 gives results for the mean separation and reattachment locations, while Fig. 5 shows velocity and turbulence/SGS-viscosity profiles, both at $x/h=2$ (roughly in the middle of the recirculation zone). The hybrid method gives the correct separation point, but predicts an excessively long recirculation zone, a defect also observed in earlier applications of the method in combination with a one-equation model in the near-wall layer (Hanjalić et al., 2003; Temmerman et al., 2005). The log-law-based wall function returns a seriously delayed separation and premature reattachment, a result also reported in Temmerman et al. (2002). Finally, the two-layer method, here operating with $F_i=\frac{\partial p}{\partial x_i}$ for reasons stated earlier, also predicts late separation, but the reattachment location agrees fairly well with that of the fully-resolved simulation. Reference to the velocity profiles reveals that all calculations, but that with the wall function, agree reasonably well with the reference solution. Two particularly encouraging features are, first, that the two-layer model, which is an especially simple and economical implementation, gives a significantly superior representation to that of the wall-function, and second, that the results of the hybrid model are fairly insensitive to the location of the interface. As seen from the profiles of turbulence/SGS viscosity, increasing the thickness of the near-wall layer leads, as expected, to a steep rise in the turbulence activity represented by the statistical model; yet, the quality of the result obtained from the simulation does not deteriorate.

5. Hydrofoil flow

This separated flow evolves along an asymmetric trailing edge of a model hydrofoil, as shown in Fig. 6. The Reynolds number, based on the free stream velocity U_∞ and the hydrofoil chord, is 2.15×10^6. The corresponding Reynolds number, based on hydrofoil thickness, is 101,000. Simulations were performed over the rear-most 38% of the hydrofoil chord with inlet conditions discussed below. The flow had previously been investigated experimentally by Blake (1975) and numerically by Wang and Moin (2000). The computational domain is $0.5H\times41H\times16.5H$, where H denotes the hydrofoil thickness. Table 3 lists the simulations performed. The present 'coarse-grid' results are compared to those obtained by Wang and Moin (2002) on a C-grid of $1536\times96\times48$ nodes, claimed to be well-resolved. In the two-layer implementation, the distance, in wall units, between the wall-nearest LES grid node and the wall, in the straight portion of the hydrofoil, is $y^+=40$, while in the case of the hybrid scheme, the interface is at $y^+=60$ and 120 for the simulations denoted with $j12$ and $j19$, respectively. The choice of a thinner near-wall layer for the two-layer implementation, relative to the hybrid scheme, reflects the recognition that this approach poses limitations not dissimilar to those of wall-functions, especially in non-equilibrium regions close to or within separated zones. The inter-nodal distance in both streamwise and spanwise directions is $\Delta x^+=120$, again applicable to the boundary-layer portion upstream of the trailing-edge region. Note that the two-layer grid contains only one quarter of the number of nodes of that used for the reference simulation.

Inflow-boundary conditions were taken from Wang and Moin (2002). These were generated in two parts: first, an auxiliary RANS calculation was performed over the full hydrofoil, using the k–$v2f$ turbulence model of Durbin (1995); the unsteady inflow data were then generated from two separate precursor LES computations for flat-plate boundary layers at zero pressure gradient. Discrete time series of the three velocity components at the appropriate spanwise (y–z) plane were then saved. These data, appropriately interpolated, were fed into the inflow boundaries of the present simulations. The upper and lower boundaries are located at 41 hydrofoil thicknesses away from the wall, so as to minimize numerical blocking effects. At the downstream boundary, conventional convective outflow conditions are applied.

Results given in Figs. 6 and 7 convey the performance of the two-layer method relative to the log-law-based wall-function implementation and the reference solution. Fig. 6 gives wall-normal profiles of the mean-velocity magnitude, $U=(U^2+V^2)^{\frac{1}{2}}$, and of streamwise rms velocity along the hydrofoil (U_e is the boundary-layer-edge veloc-

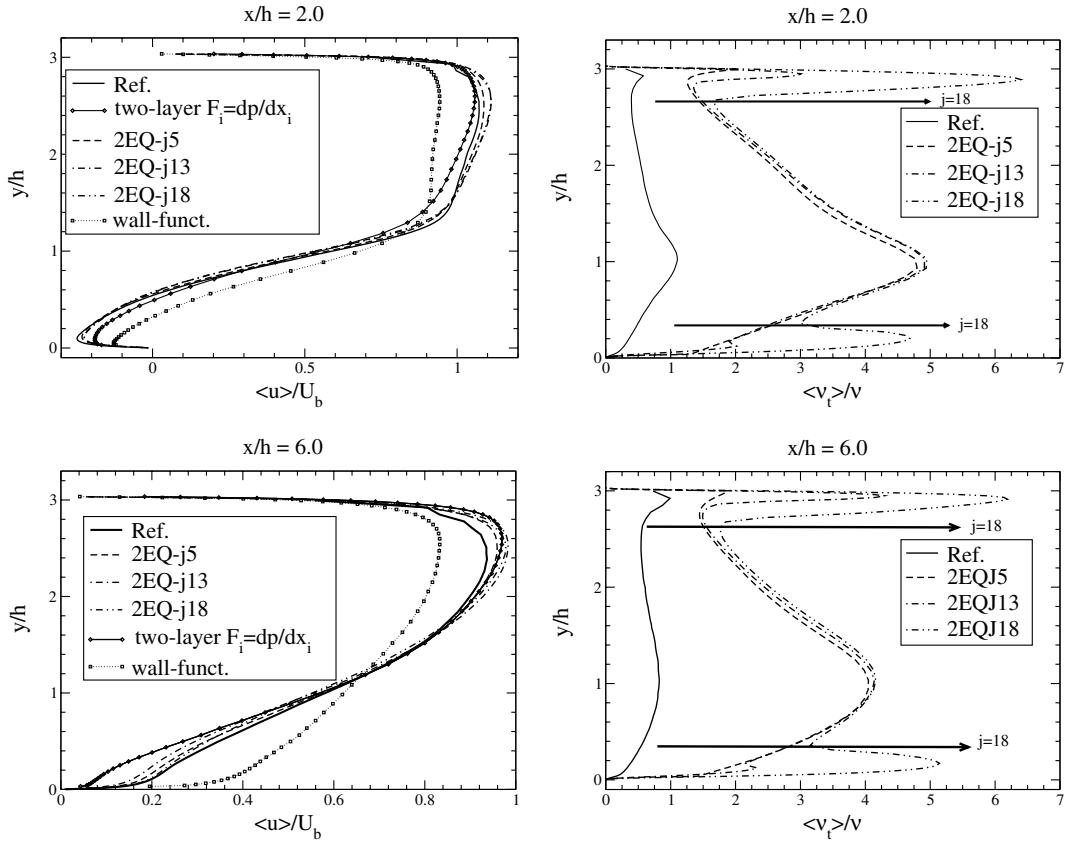

Fig. 5. Profiles of velocity (left-hand side) and turbulent/SGS-viscosity (right-hand side) for periodically constricted channel flow at $Re = 21{,}560$; Ref. LES with $196 \times 128 \times 186$ nodes, relative to $112 \times 64 \times 56$ for the RANS/LES hybrid and $112 \times 64 \times 56$ for the two-layer approximations.

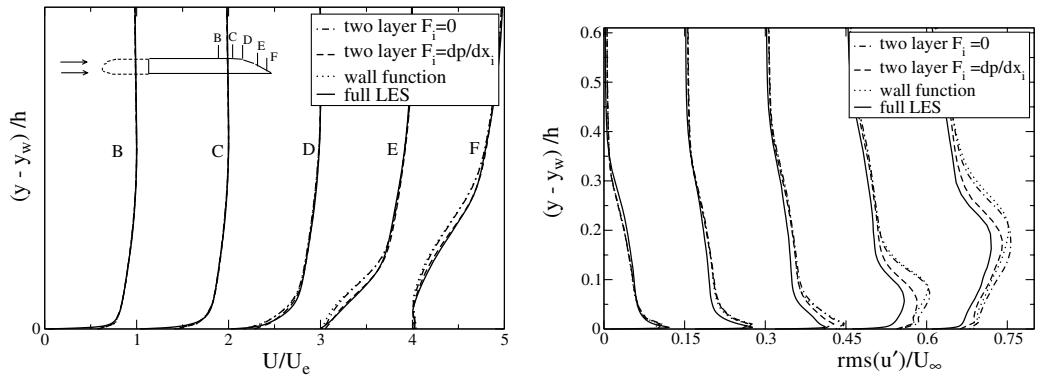

Fig. 6. Profiles on mean-velocity magnitude (left-hand side), and rms of streamwise velocity (right-hand side) at $x/H = -3.125$ (B), -2.125 (C), -1.625 (D), -1.125 (E), -0.625 (F).

Table 3
Grids, modelling practices and interface locations for hydrofoil simulations

Case	Grid	SGS model	Interface (y^+)
Ref. LES	$1536 \times 48 \times 96$ (C grid)	Dynamic	–
Two-layer $F_i = \frac{\partial p}{\partial x_i}$	$512 \times 128 \times 24$	Dynamic	40
Two-layer $F_i = 0$	$512 \times 128 \times 24$	Dynamic	40
2EQ-*j*12	$512 \times 128 \times 24$	*k*-eq	60
2EQ-*j*19	$512 \times 128 \times 24$	*k*-eq	120
log-Law WF	$512 \times 128 \times 24$	Dynamic	40

ity). The streamwise locations at which profiles are given are identified by 'B'–'F' in the inset of Fig. 6. Agreement is good for all the simulations in the first two sections, which are located in the straight part of the hydrofoil over which the flow is attached. Starting from section *D*, $x/H = -1.625$, the wall-function and the two-layer method with $F_i = 0$ present velocity profiles that differ from the reference simulation and from the implementation with $F_i = \frac{\partial p}{\partial x_i}$. In sections *D*, *E* and *F*, the flow field is affected by a strong pressure gradient that is not accounted for in

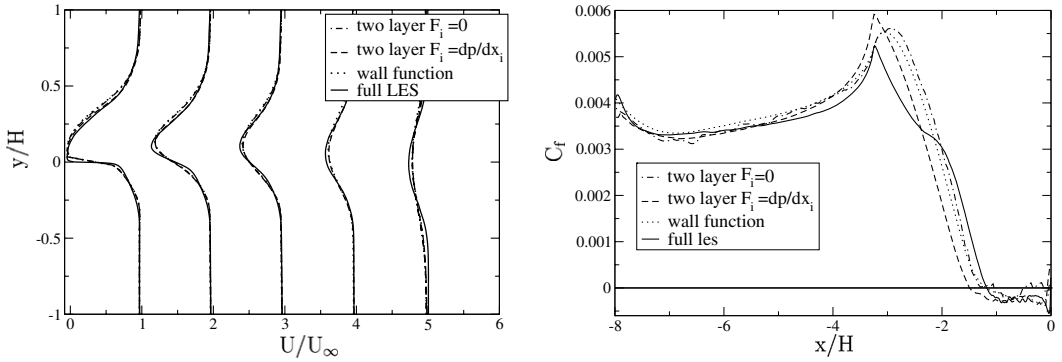

Fig. 7. Profiles of mean streamwise velocity in the wake at $x/H = 0,0.5, 1.0, 2.0$ and 4.0 (left-hand side) and distributions of mean skin-friction coefficient C_f (right-hand side).

the simplest version of the two-layer approach ($F_i = 0$). As regards the rms value of the streamwise-velocity fluctuations, the wall-function approach again gives essentially the same result as the simplified wall model. The implementation with $F_i = \frac{\partial p}{\partial x_i}$ predicts well the location of rms peak in all sections, but the actual value is too high, perhaps reflecting the weakness of the quasi-steady assumption upon which the simplified form of F_i is based. Notwithstanding order-of-magnitude considerations, it is arguable, in particular, that the inclusion of the pressure gradient should go hand-in-hand with the inclusion of advection, especially the unsteady term, for the response to a pressure gradient is not merely an increase in frictional stress, but also an acceleration or deceleration. Thus, the effect of the pressure gradient, if included on its own, may well be excessive. The extension of the two-layer model in the sense discussed above is being pursued at the time of writing. A major penalty for such an extension is, however, a significant increase in resource requirements.

Fig. 7 gives profiles of the normalized mean-streamwise velocity in the wake of the hydrofoil. The peaky feature predicted in the first profile at the hydrofoil trailing edge ($x/H = 0$) is caused by the rather coarse mesh resolution in the wall-normal direction, a consequence of the use of the H-topology in which the single-cell near-wall layers merge in the wake region and extend to the exit plane. This could be circumvented with a C-topology grid, but a resolution penalty would then arise further downstream. With respect to the skin-friction data for the upper surface, given in the right-hand-side plot of Fig. 7, it is noted first that the abrupt change in the distribution of the reference LES solution reflects the sudden change in surface curvature at the junction of the plane and the curved parts of the surface. At this junction, there is also a fairly abrupt change in the pressure gradient, and this explains the sensitivity of the results to the inclusion or exclusion of the gradient in the two-layer formulation: as seen, the inclusion of the pressure gradient leads to the sharp peak in C_f being reproduced. With this difference aside, the overall agreement achieved between all the approximations, particularly that including the pressure gradient, and the LES solution is encouraging—indeed, surprisingly good, considering the relative simplicity of the methods. The simplest two-layer variant, which excludes the pressure-gradient term, gives distributions for all quantities, which are close to those derived from the wall-function approach. This is the expected behaviour, for the former is constrained to return a solution in the near-wall layer that complies with the log law, which is imposed explicitly within the wall-function formulation. The inclusion of the pressure gradient causes an early separation relative to the LES result, as observed by reference to the skin-friction distributions. However, the

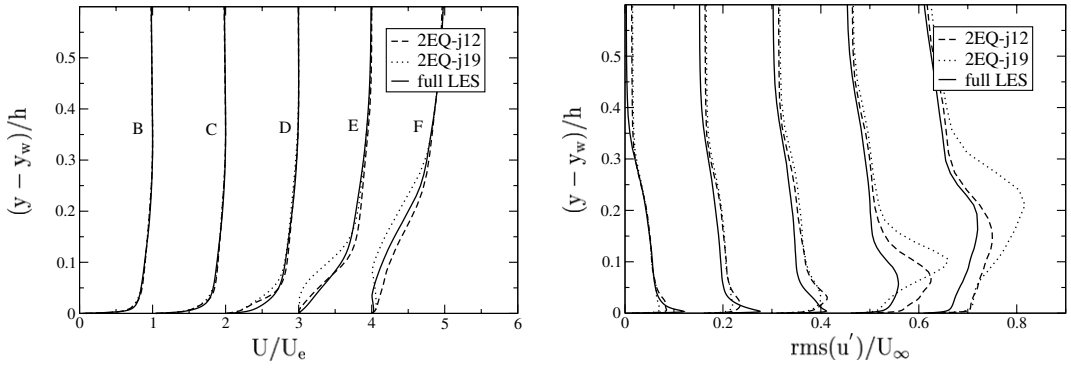

Fig. 8. Profiles of mean-velocity magnitude (left-hand side) and rms of streamwise velocity (right-hand side) at $x/H = -3.125, -2.125, -1.625, -1.125$ and -0.625.

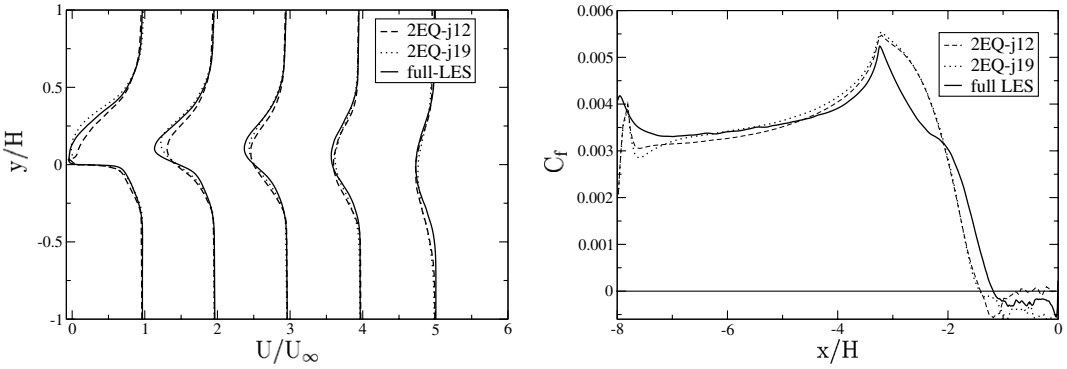

Fig. 9. Profiles of the mean streamwise velocity in the wake at $x/H = 0{,}0.5$, 1.0, 2.0 and 4.0 (left-hand side) and mean skin-friction coefficient C_f (right-hand side).

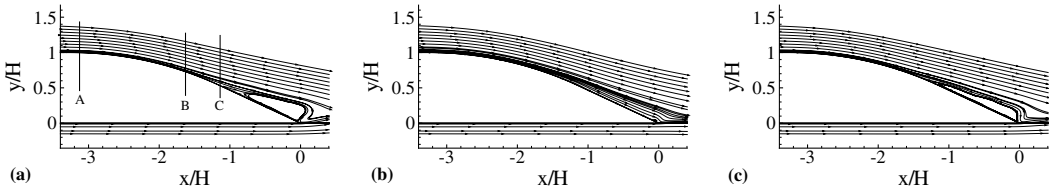

Fig. 10. Streamline patterns close to the trailing edge of the hydrofoil; (a) two-layer model $F_i = \frac{\partial p}{\partial x_i}$; (b) two-equations hybrid model 2eq $- j12$; (c) two-equations hybrid model 2eq $- j19$.

velocity profiles at E and F, given in Fig. 6, agree closely with the reference LES. Hence, there appears to be a degree of inconsistency in the predictive quality of the skin friction and the flow field, implying that the recirculation zone predicted by the approximate schemes develops at a different rate than that predicted by the LES and recovers more quickly. As a consequence, when the flow reaches location E, the premature separation predicted with the pressure gradient included is not detectable and agreement is close. Conversely, when a broadly correct separation location is predicted, the recirculation zone is thicker than it should be at locations E and F.

Figs. 8 and 9 present results obtained with the hybrid strategy, corresponding to Figs. 6 and 7 discussed earlier. An immediate observation is that the quality of the solutions is materially sensitive to the details of the simulations. To aid the interpretation of this sensitivity, Fig. 10 shows time-averaged streamfunction fields above the trailing edge, while Fig. 11 shows the numerical grid with the interfaces at $y^+ = 60$ and 120 and profiles of turbulent viscosity at three streamwise locations, namely 'A', 'B' and 'C'. With respect to the skin friction data, it is noted first that the hybrid scheme with the interface at $j = 12$ predicts a short separation zone, but returns the flow, wrongly, to a marginally attached state, in contrast to the reference and two-layer solutions. Consistently, Fig. 10(b) shows a thin recirculation zone at around $x/H = -1.3$, followed by an attached flow. This is a behaviour normally anticipated to be produced by an overly diffusive RANS model. An important feature of the mesh to be highlight in respect of this particular simulation is the high mesh-aspect ratio above the interface, i.e. in the LES region. This feature is highly disadvantageous to the accuracy of the LES and an inevitable consequence of the proximity of the interface to the wall in the region where the mesh needs to be progressively refined at a gentle rate towards the wall. In this respect, the present case shows that the insensitivity of the results to the location of the interface observed for the channel flow does not necessarily carry over to more complex separated flow. That the hybrid scheme performs as desired, at least in principle, is demonstrated by the fact that the turbulent viscosity rises sharply within the near-wall layer, a behaviour entirely in accord with that shown earlier for the 2d-hill flow, Fig. 5. As seen in Fig. 10, placing the interface at $j = 19$, a choice that returns the cell-aspect ratio to a level more appropriate for LES, results in the hybrid scheme predicting a substantial separation zone above the trailing edge. At the same time, C_f drops to negative values broadly consistent with the reference solution. Moreover, Fig. 11 demonstrates that shifting the interface away from the wall increases substantially the eddy viscosity in the near-wall layer, again in line with expectations. In contrast to these positive features, Fig. 8 shows that the structure of the near-wall flow, within the layer of thickness 0.2 times the trailing-edge thickness, is poorly predicted. In particular, there is an excessive outward displacement of the separated shear, with the position of maximum resolved rms value at location 'F' ($x/H = -0.625$) being at $(y - y_w)/h = 0.22$, rather than 0.15 (note the expanded scale of the ordinate relative to the streamwise geometry of the trailing edge, shown in Fig. 10). Moreover, the turbulence intensity is excessive,

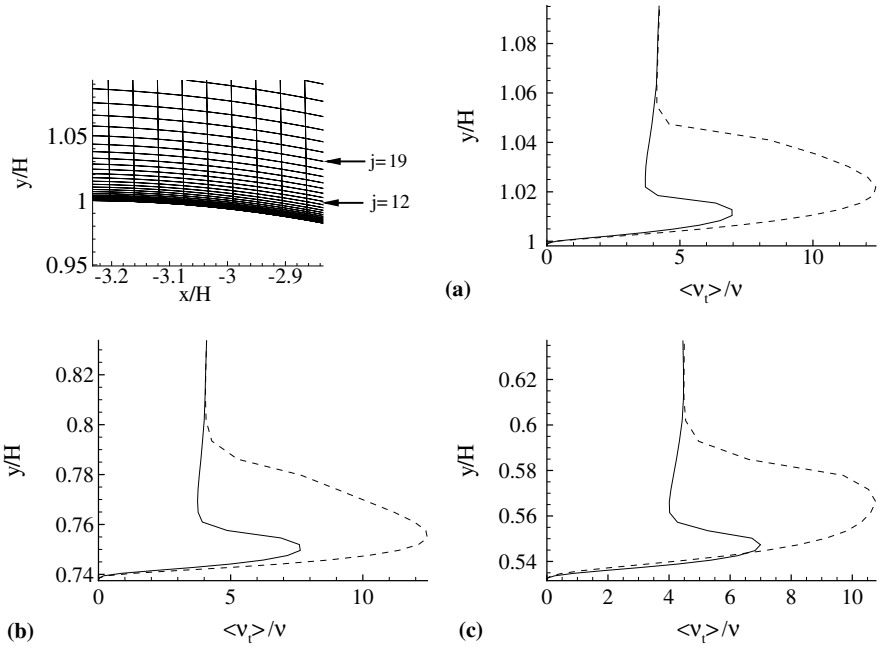

Fig. 11. Ratio of turbulent viscosity to fluid viscosity above the upper side of the hydrofoil at the locations $x/H = -3.125$ (a), -1.625 (b), -1.125 (c). (——) Two-equations hybrid model $j = 12$, (-----) two-equation hybrid model $j = 19$. The interface locations $j = 12$, 19 are identified in the upper left-hand-side plot of the suction-side grid, around $x/H = -3.0$.

but this is mainly a reflection of too early separation and more vigorous turbulence activity resulting from the shear layer being too far from the wall. Close examination of the near-wall region ahead of separation shows the resolved turbulence level to be substantially lower than that of the reference computation. While this is expected, in view of the RANS viscosity being high in this region, it seems that the total shear stress in the boundary layer is too low, thus leading to premature separation. A further feature deserving consideration is the rapid decline in turbulent viscosity as the interface is approached away from the wall. This reduction reflects the constraint that the turbulent viscosity should be continuous at the interface. In this region, it is likely that the diminution of the modelled component of turbulence is not matched by a commensurate rise in the resolved activity, so that the total level of turbulence is too low. This then leads to an excessive tendency towards separation and too high strain rate, as is observed in Fig. 9.

6. Concluding remarks

No approximation of the near-wall region within a LES scheme that sacrifices full resolution will give an entirely satisfactory representation of this region, and this statement also applies to the methodologies investigated in the present paper. The overall objective can only be to devise a method that will allow the simulation to maintain an adequate predictive realism in the outer flow and, thus returning an acceptable accuracy of the gross flow features.

Of the two methods examined, the hybrid approach is more expensive, but allows the interface to be placed further away from the wall and to provides a numerically consistent framework. In channel flow, the method was shown to yields results which are only weakly dependent on the location of the interface—within reasonable limits, of course. However, in the much more complex trailing-edge flow, the solution is considerably more sensitive to the interface location, and this is a cause of some concern that needs to be explored further. In particular, it seems that the aspect ratio of the cells on the LES-side of the interface is an influential issue that needs to be examined. Relative to the earlier use of one-equation modelling in the near-wall layer, two-equation modelling does not seem to offer decisive benefits. Whatever model is adopted, small-scale (high-frequency) information is progressively lost as the near-wall layer is thickened, and this may require to be compensated for by some form of spectral enrichment (see, for example, Hanjalić et al., 2003).

The principal attraction of the zonal two-layer strategy lies in its economy and simplicity. It is, essentially, a method for generating, numerically, a solution in the near-wall layer, which is an improvement on the analytically prescribed log-law-based wall function. In fact, the two are virtually equivalent for $F_i = 0$ in Eq. (6). Inclusion of the pressure gradient in F_i is found to yield improvements, and the results presented for all three flows are clearly encouraging. On the other hand, the method does not allow thick near-wall layers to be prescribed without significant errors being provoked due to a serious deterioration in resolution. This also applies to wall-law-based approaches. Finally, it is arguable that the quasi-steady implementation, in which F_i in Eq. (6) only contains the pressure gradient, is too simple. This may be appreciated upon noting that fluctuations in pressure gradient are bal-

anced, at least to some extent, by inertial perturbations, even close to the wall. It thus follows that the transport terms need to be included in F_i, which brings about a significant complication of the algorithm, with attendant cost implications. This is the subject of ongoing efforts.

Acknowledgements

This work was undertaken, in part, within the DESider project (Detached Eddy Simulation for Industrial Aerodynamics), a collaboration between ALA, CFX, DASSAV, EADS-M, ECD, LML, NLR, EDF, NUMECA, DLR, FOI, IMFT, ONERA, Chalmers University, Imperial College, TU Berlin, UMIST and NTS. The project is funded by the European Union and administrated by the CEC, Research Directorate-General, Growth Programme, under Contract No. AST3-CT-2003-502842.

References

Balaras, E., Benocci, C., 1994. Subgrid-scale models in finite difference simulations of complex wall bounded flows. In: Applications of Direct and Large Eddy Simulation. AGARD CP551, pp. 2-1–2-6.

Balaras, E., Benocci, C., Piomelli, U., 1996. Two-layer approximate boundary conditions for large-eddy simulations. AIAA J. 34 (6), 1111–1119.

Blake, W.K., 1975. A statistical description of pressure and velocity fields at the trailing edge of a flat structure. DTNSRDC Report 4241, David Taylor Naval Ship R&D Center, Berthesda, MD.

Cabot, W., 1995. Large-eddy simulations with wall-models. Tech. Rep. Annual Research Briefs, Center for Turbulence Research, Stanford, USA.

Dahlström, S., 2003. Large eddy simulation of the flow around a high-lift airfoil. Ph.D. Thesis, Chalmers, Göteborg, Sweden.

Durbin, P., 1995. Separated flow computations with the k–epsilon–$v2$ model. AIAA J. 33 (4), 659–664.

Germano, M., Piomelli, U., Moin, P., Cabot, W., 1991. A dynamic subgrid-scale eddy viscosity model. Phys. Fluids A 3 (7), 1760–1765.

Hamba, F., 2001. An attempt to combine large eddy simulation with the k–ϵ model in a channel flow computation. Theor. Comput. Fluid Dyn. 14 (5), 323–326.

Hanjalić, K., Hadziabdić, M., Temmerman, L., Leschziner, M., 2003. Merging LES and RANS strategies: zonal or seamless coupling? In: Friedrich, R., Geurts, J., Métais, O. (Eds.), Direct and Large Eddy Simulations V. Kluwer Academic Press, pp. 451–464.

Lien, F., Leschziner, M., 1994. A general non-orthogonal collocated finite volume algorithm for turbulent flow at all speeds incorporating second-moment turbulence-transport closure. Part 1: computational implementation. Comput. Methods Appl. Mech. Eng. 114, 123–148.

Nicoud, F., Ducros, F., 1999. Subgrid-scale stress modelling based on the square of the velocity gradient tensor. Flow Turbul. Combust. 62 (3), 183–200.

Shur, M., Spalart, P., Strelets, M., Travin, A., 1999. Detached-eddy simulation of an airfoil at high angle of attack. In: Rodi, W., Laurence, D. (Eds.), Engineering Turbulence Modelling and Experiments 4. Elsevier Science, Amsterdam, pp. 669–678.

Spalart, P., 2000. Strategies for turbulence modeling and simulations. Int. J. Heat Fluid Flow 21 (3), 252–263.

Temmerman, L., Leschziner, M., Hanjalić, K., 2002. A-priori studies of a near-wall RANS model within a hybrid LES/RANS scheme. In: Rodi, W., Fueyo, N. (Eds.), Engineering Turbulence Modelling and Experiments V. Elsevier, Amsterdam, pp. 317–326.

Temmerman, L., Leschziner, M., Mellen, C.P., Fröhlich, J., 2003. Investigation of wall-function approximations and subgrid-scale models in large eddy simulation of separated flow in a channel with streamwise periodic constrictions. Int. J. Heat Fluid Flow 24 (2), 157–180.

Temmerman, L., Hadziabdić, M., Leschziner, M., Hanjalić, K., 2005. A hybrid two-layer URANS–LES approach for large eddy simulation at high Reynolds numbers. Int. J. Heat Fluid Flow 26 (2), 173–190.

Wang, M., Moin, P., 2000. Computation of trailing-edge flow and noise using large-eddy simulation. AIAA J. 38 (12), 2201–2209.

Wang, M., Moin, P., 2002. Dynamic wall modelling for large-eddy simulation of complex turbulent flows. Phys. Fluids 14 (7), 2043–2051.

Wray, A., 1998. Decaying isotropic turbulence. Tech. Rep. 345, Agard.

Yoshizawa, W., Horiuti, K., 1985. A statistically derived subgrid scale kinetic energy model for the large eddy simulation of turbulent flows. J. Phys. Soc. Jpn. 54 (8), 2834–2839.